The Axial Tyrosinate Fe^{3+} Ligand in Protocatechuate 3,4-Dioxygenase Influences Substrate Binding and Product Release: Evidence for New Reaction Cycle Intermediates[†,‡]

Richard W. Frazee,[§] Allen M. Orville,[∥] Kevin B. Dolbeare, Hong Yu, Douglas H. Ohlendorf, and John D. Lipscomb*

Department of Biochemistry, Medical School, and Center for Metals in Biocatalysis, University of Minnesota, Minneapolis, Minnesota 55455

Received August 19, 1997; Revised Manuscript Received December 9, 1997

ABSTRACT: The essential active site Fe^{3+} of protocatechuate 3,4-dioxygenase [3,4-PCD, subunit structure $(\alpha\beta Fe^{3+})_{12}$] is bound by axial ligands, Tyr447 (147β) and His462 (162β), and equatorial ligands, Tyr408 (108β), His460 (160β), and a solvent OH^- (Wat827). Recent X-ray crystallographic studies have shown that Tyr447 is dissociated from the Fe^{3+} in the anaerobic 3,4-PCD complex with protocatechuate (PCA) [Orville, A. M., Lipscomb, J. D., and Ohlendorf, D. H. (1997) *Biochemistry 36*, 10052−10066]. The importance of Tyr447 to catalysis is investigated here by site-directed mutation of this residue to His (Y447H), the first such mutation reported for an aromatic ring cleavage dioxygenase containing Fe^{3+}. The crystal structure of Y447H (2.1 Å resolution, *R*-factor of 0.181) is essentially unchanged from that of the native enzyme outside of the active site region. The side chain position of His447 is stabilized by a $His447^{N\delta1}$−$Pro448^{O}$ hydrogen bond, placing the Nϵ2 atom of His447 out of bonding distance of the iron (∼4.3 Å). Wat827 appears to be replaced by a CO_3^{2-}, thereby retaining the overall charge neutrality and coordination number of the Fe^{3+} center. Quantitative metal and amino acid analysis shows that Y447H binds Fe^{3+} in ∼10 of the 12 active sites of 3,4-PCD, but its k_{cat} is nearly 600-fold lower than that of the native enzyme. Single-turnover kinetic analysis of the Y447H-catalyzed reaction reveals that slow substrate binding accounts for the decreased k_{cat}. Three new kinetically competent intermediates in this process are revealed. Similarly, the product dissociation from Y447H is slow and occurs in two resolved steps, including a previously unreported intermediate. The final E·PCA complex (ES_4) and the putative E·product complex (ESO_2*) are found to have optical spectra that are indistinguishable from those of the analogous intermediates of the wild-type enzyme cycle, while all of the other observed intermediates have novel spectra. Once the E·S complex is formed, reaction with O_2 is fast. These results suggest that dissociation of Tyr447 occurs during turnover of 3,4-PCD and is important in the substrate binding and product release processes. Once Tyr447 is removed from the Fe^{3+} in the final E·PCA complex by either dissociation or mutagenesis, the O_2 attack and insertion steps proceed efficiently, suggesting that Tyr447 does not have a large role in this phase of the reaction. This study demonstrates a novel role for Tyr in a biological system and allows evaluation and refinement of the proposed Fe^{3+} dioxygenase mechanism.

Protocatechuate 3,4-dioxygenase (EC 1.13.11.3) (3,4-PCD)[1] catalyzes the cleavage of O_2 and concomitant ring opening of protocatechuate (3,4-dihydroxybenzoate, PCA) to yield β-carboxy-*cis*,*cis*-muconate (β-CM) which contains both oxygen atoms from O_2 (for a review, see ref *1*). The enzyme has been the most thoroughly studied enzyme of the intradiol-cleaving catecholic dioxygenase class. 3,4-PCD enzymes isolated from at least 10 different classes of bacteria have been shown to be composed of between 4 and 12 protomers, each with an $\alpha\beta Fe^{3+}$ subunit structure. Extensive spectroscopic studies (for reviews, see refs *1*−*4*) of several of the enzymes and crystallographic studies (*5*, *6*) of the enzyme isolated from *Pseudomonas putida* (formerly classified as *Pseudomonas aeruginosa*[2]) have shown that the iron is bound in the β subunit in a five-coordinate trigonal bipyramidal ligand environment with Tyr447[3] and His462 as the axial ligands and Tyr408, His460, and a OH^-

[†] This work was supported by National Institutes of Health Grants GM-24689 to J.D.L. and GM-46436 to D.H.O. National Institutes of Health Training Grants GM-08277, GM-07323, and GM-08347 provided partial support for R.W.F., A.M.O., and K.B.D., respectively.

[‡] The coordinates for the Y447H mutant form of 3,4-PCD have been submitted to the Brookhaven Protein Data Bank under identification code 3PCD.

* Corresponding author: 4-225 Millard Hall, Department of Biochemistry, University of Minnesota, Minneapolis, MN 55455-0347. Telephone: (612) 625-6454. Fax: (612) 625-2163. E-mail: lipsc001@maroon.tc.umn.edu.

[§] Current address: Department of Chemistry, The University of Michigan−Flint, Flint, MI 48502.

[∥] Current address: Institute of Molecular Biology, University of Oregon, Eugene, OR 97403.

[1] Abbreviations: 3,4-PCD, protocatechuate 3,4-dioxygenase; PCA, protocatechuate or 3,4-dihydroxybenzoate; β-CM, β-carboxy-*cis*,*cis*-muconate; INO, 2-hydroxyisonicotinic acid *N*-oxide; NNO, 6-hydroxynicotinic acid *N*-oxide; EPR, electron paramagnetic resonance; EXAFS, extended X-ray absorption fine structure; LMCT, ligand to metal charge transfer; rms, root-mean-squared; TB, terrific broth.

[2] American Type Culture Collection (ATCC) 23975, previously classified as *P. aeruginosa*.

S0006-2960(97)02047-3 CCC: $15.00 © 1998 American Chemical Society
Published on Web 02/06/1998

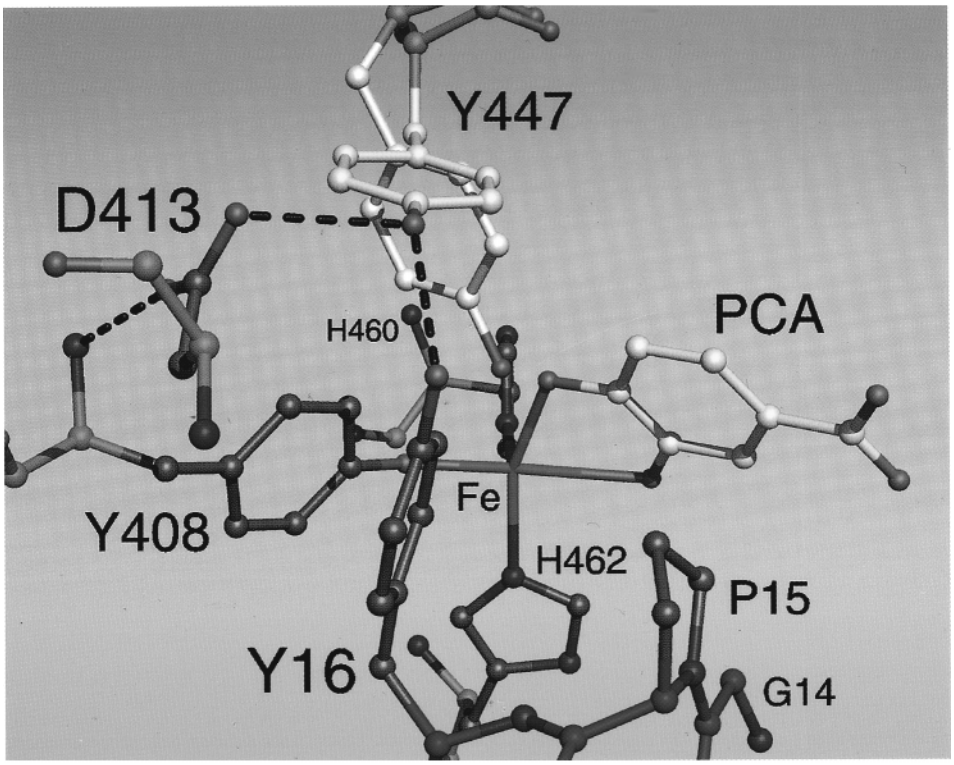

FIGURE 1: Structure of the active site region of 3,4-PCD with PCA bound from crystallographic studies (*7*). Shown in white for reference is the position of Tyr447 in the active site structure determined in the absence of PCA (*6*). Backbone carbon atoms from the α and *β* subunits are colored red and green, respectively. Prepared with MIDAS+ (*8*), from the Computer Graphics Laboratory of the University of California, San Francisco (supported by NIH Grant RR-01081).

(Wat827) as the equatorial ligands (Figure 1). The burgundy color of the enzyme is a consequence of ligand to metal charge transfer (LMCT) from the tyrosinate ligands to the iron (reviewed in refs *2* and *3*). The optical spectrum is relatively broad because Tyr408 and Tyr447 contribute discrete LMCT bands at about 435 and 525 nm, respectively (*9*). Wat827 extends into the active site and is displaced by substrates and some inhibitors as they bind to the enzyme and the iron.

As illustrated in Figure 1, our recent crystallographic studies of a range of inhibitor and substrate complexes of 3,4-PCD show that substrate binds as an Fe^{3+} chelate, displacing the equatorial OH^- and axial Tyr447 ligands (*7*, *10*, *11*). The displaced ligands are both anions and appear to function as active site bases to facilitate deprotonation of PCA so that it can bind to the Fe^{3+} in the dianionic state, thereby maintaining the zero net charge of the iron center. The binding of substrate also converts the iron coordination geometry to five-coordinate octahedral with a vacant site in the equatorial plane adjacent to the substrate binding site. The crystal structures of several monohydroxybenzoate inhibitor complexes of 3,4-PCD revealed many possible binding orientations for substrate-like molecules in the active site, but no displacement of the axial Tyr447. Viewed together, these inhibitor and substrate complex structures provide structural models for a reasonable series of steps in the substrate binding process. Substrate is postulated to enter the active site to form a weak complex away from the iron, and then form a monodentate complex with the iron through the C4-phenolate group, thereby displacing or shifting Wat827 and converting the coordination geometry to octahedral. Finally, the substrate is thought to shift to a chelate structure in which the C4-O^- displaces Tyr447 from an axial ligation site, the C3-OH is deprotonated and binds in the equatorial plane, and solvent is displaced if it remained bound in the previous step.

There are relatively few well-characterized examples of the displacement of an endogenous ligand in metalloproteins. The structurally defined examples include (i) the carboxylate shift observed in binuclear iron enzymes such as ribonucleotide reductase and methane monooxygenase (reviewed in refs *12* and *13*), (ii) dissociation of the oxo ligand and the shift of the dithiolene S ligands to the molybdopterin cofactor within dimethyl sulfoxide reductase upon two-electron reduction (*14*), (iii) expansion of the iron coordination sphere in iron superoxide dismutase upon azide (a substrate analogue) binding (*15*), (iv) displacement of Gln330 from the coordination by substrate binding to the Fe^{2+} of isopenicillin *N*-synthase (*16*), and (v) the ligand switching at both hemes of cytochrome cd_1 nitrite reductase during catalysis (*17*, *18*). However, 3,4-PCD, perhaps better than the other examples, defines the role of exogenous ligand binding in the alteration of the iron coordination sphere and correlates these to the function of the enzyme.

The displacement of Tyr447 in 3,4-PCD upon substrate binding in the enzyme−substrate complex at equilibrium raises the question of whether this displacement occurs during catalysis. One way to test this is to characterize the enzyme structure and catalytic properties after replacing Tyr447 with other amino acids by site-directed mutagenesis. Although random mutagenesis has been successfully applied to 3,4-

[3] The amino acid residue numbering scheme is from the refined structure of 3,4-PCD as isolated from *P. putida* (*6*): α subunit (residues 1−200) and *β* subunit (residues 301−538).

PCD isolated from *Acinetobacter calcoaceticus* (*19*), site-directed mutagenesis and characterization of the recombinant mutant forms have not been reported. We recently cloned, sequenced, and overexpressed the 3,4-PCD from *P. putida* (*20*). Physical, spectroscopic, and kinetic characterization showed that this recombinant 3,4-PCD is essentially indistinguishable from the natural enzyme, showing that this is an excellent system in which to pursue site-directed mutagenesis studies.

Here we describe the first construction and extensive characterization of a site-directed mutant for an Fe^{3+}-containing aromatic ring-cleaving dioxygenase. It is shown that exchange of histidine for Tyr447 causes little change in the overall structure of the enzyme, but it does dramatically alter the spectra and catalytic parameters of 3,4-PCD. Evaluation of the transient kinetics of turnover as well as the spectra of both the substrate complex and the reaction cycle intermediate complexes suggests that the major catalytic changes occur in the substrate association and product release phases of the catalytic cycle. The oxygen insertion reaction itself appears to remain relatively unaffected, consistent with the proposal that the ligand in question is displaced during the oxygen insertion steps of the cycle. Several new intermediates of the catalytic cycle are revealed due to the decrease in the rate of the substrate binding and product release processes. These intermediates are consistent with the stepwise substrate binding process suggested by the structural studies of inhibitor complexes described above.

EXPERIMENTAL PROCEDURES

Chemicals and Standard Procedures. All chemicals used were reagent grade quality or better and were obtained from either Sigma or Aldrich Inc. Protocatechuate (PCA) was recrystallized from distilled water and dried under a vacuum in a sealed desiccator. Glass-distilled water was used in all buffers, while water treated by reverse osmosis was used in the growth media. Anaerobic sample handling techniques have been described previously (*21*).

Strains and Plasmids. All recombinant expression was performed in *Pseudomonas fluorescens* ATCC 17557. *Escherichia coli* JM109 has the genotype *endA1 recA1 gyr96 thi hsdR17*(r_K^-, m_K^+) *relA1 supE44* λ^- Δ (*lac-proAB*) [F′ *traD36 proA*$^+$*B*$^+$ *lacI*^{q} ZΔM15]. *E. coli* RR1 has the genotype F$^-$ *mcrB mrr hsdS20*(r_B^- m_B^-) *leuB6 recA hisB ara-14 proA2 lacY1 galK2 xyl-5 mtl-1 rpsL20*(sm^r) *supE44* λ^- (*22*). *E. coli* ECY5058 is strain HB101 (*hsd20 recA13 proA2 leuB6 thi-1*) (*23*) carrying pRK2013 (*24*). *E. coli* BMH 71−18 *mut*S has the genotype *thi supE* Δ (*lac-proAB*) [*mutS*::Tn10] [F′ *proA*$^+$*B*$^+$ *lacI*^{q} ZΔM15].

Plasmid pKMY319 was kindly provided by K.-M. Yen of Amgen Corp. (*25*). Plasmid pRWF115 and the expression vector for 3,4-PCD, pRWF113, were constructed as previously described (*20*). Plasmid pALTER-1 was purchased from Promega as part of the "Altered Sites Mutagenesis" kit.

Culture Conditions. All *E. coli* strains were grown in Luria broth (LB) at 37 °C. *Pseudomonas fluorescens* (ATCC 17557) was grown in either LB or Hutner's minimal media (*26*) supplemented with 1% glucose at 30 °C. Antibiotics were used in selection media at the following concentrations: ampicillin, 150 μg/mL; kanamycin, 50 μg/mL; and tetracycline, 15 μg/mL for pALTER derivatives, 25 μg/mL for pKMY319 derivatives in *E. coli*, or 150 μg/mL in *P. fluorescens*. Lactose phenotypes were screened as previously described (*20*).

Transformations and matings were as previously described (*20*) except that transconjugants were selected at 30 °C on Hutner's minimal media supplemented with 0.2% glucose and 150 μg/mL tetracycline.

Site-Directed Mutagenesis. The procedures used for cloning and plasmid manipulations were as previously described (*20*). Restriction endonucleases and modifying enzymes were supplied by New England Biolabs and Promega. All restriction digests and DNA modifications were carried out as recommended by the supplier. All mutants were made using the Altered Sites kit purchased from Promega Inc., following the manufacturer's protocol. The pALTER-1 plasmid was engineered to produce a *Bst*EII site in the SP6 promoter just downstream of the multiple cloning site using an oligonucleotide having the sequence 5′-CTTGAGTATTCTATAGGGTGACCTAAATAGCTTG-3′. Positive clones were identified by digestion with *Bst*EII. One clone, containing both ampicillin and tetracycline resistance as well as the *Bst*EII site, was designated pRWF117. The *Bst*EII-containing 470 bp *Cla*I−*Pst*I fragment from pRWF117 was cloned back into pALTER-1, creating pRWF119. Plasmid pRWF120, the template for mutagenesis, was constructed by cloning the *Bst*EII−*Sal*I fragment from pRWF115 into pRWF119.

The Y447H mutant was made using pRWF120 and an oligonucleotide having the sequence 5′-GCCGGGCCCG-**C**ACCCCTGGCG-3′ which is complementary to the non-coding strand except at the single base mutation in the tyrosine codon, TAC. Potential mutants were screened by sequencing the DNA as described below (see DNA Sequencing). A clone, designated pRWF133, containing the desired mutation was completely sequenced over the *Bst*EII−*Sal*I region to ensure that secondary mutations were not introduced. The *Bst*EII−*Sal*I fragment from pRWF133 was subcloned to pRWF115 in place of the wild-type fragment. A clone, containing the mutant fragment, was identified by DNA sequencing and designated pRWF156. Expression plasmid pRWF158 was constructed by cloning the *Cla*I−*Xho*I fragment from pRWF156 into the broad-host range expression plasmid pKMY319.

DNA Sequencing. Potential Y447H subclones were screened and verified using the dideoxy method of DNA sequencing (*27*) as previously described (*20*).

Western Analysis. Antibodies against 3,4-PCD were prepared by Bethyl Laboratories from dissolved crystals of *P. putida* wild-type 3,4-PCD. Cultures were grown in either terrific broth (TB, 1.2% tryptone, 2.4% yeast extract, and 70 mM KPO_4 at pH 7.0) (*28*) or Hutner's minimal media supplemented with 0.5% glucose. Salicylate was added to 0.35 mM, while *p*-hydroxybenzoate was added to 5 mM when indicated by the protocol described. Cell extracts were prepared and denatured and companion gels stained as previously described (*20*). SDS−polyacrylamide gel electrophoresis (Page) of 5−20 μL of protein extract per lane was performed using a constant voltage (200 V) via standard techniques (*29*) and a Bio-Rad Mini Protean II system at 4 °C.

Electrophoretically resolved proteins were transferred to nitrocellulose membranes, which had been pretreated with transfer buffer [25 mM Tris (pH 8.3), 192 mM glycine, and 20% methanol], at 100 V (constant) and 4 °C for 1 h. Membranes were processed as described in the Biorad goat anti-rabbit antibody horseradish peroxidase (GAR-HRP) kit. 3,4-PCD-challenged rabbit sera (IgG) was added and the mixture incubated with shaking at room temperature for 2−20 h in antibody dilution buffer (Biorad). After the mixture was treated with a blocking solution [20 mM Tris (pH 7.5), 0.5 M NaCl, and 3% gelatin], GAR-HRP was added and the mixture incubated as above. Detection of cross-reactive proteins involved incubating membranes at room temperature for 0.5 h in fresh color development solution (1× Tris-buffered saline, 0.015% H_2O_2, and 4-chloro-1-naphthol).

Growth and Expression. *P. fluorescens*, containing either pRWF113 or pRWF158, was grown in 45 L carboys containing Hutner's minimal media supplemented with 1% glucose, 150 μg/mL tetracycline, and 3.5 mM sodium salicylate. A 5 mL overnight culture of *P. fluorescens*, carrying recombinant 3,4-PCD expression constructs, was used to inoculate 1 L of the supplemented Hutner's minimal media. The culture was grown overnight to an optical density of greater than 2.0 (at 550 nm) with shaking at 30 °C. A 0.5 L volume of the culture was used to inoculate each carboy. Details of aeration, harvesting, and storage were as described previously (*20*) except that the temperature was maintained at or below 30 °C. During log phase growth, significant amounts of acidic byproducts were produced and this required frequent neutralization with 6 N NaOH.

Purification of Recombinant 3,4-PCDs. All purification steps were carried out at 4 °C. Approximately 300−500 g (wet weight) of bacteria was resuspended in 2 volumes (w/v) of buffer A [50 mM Tris-HCl (pH 8.5) and 10 mM β-mercaptoethanol]. Bacteria were disrupted by sonication as previously described (*20*); the suspension was diluted to 1 L with buffer A and centrifuged in JA-17 rotors (Beckman) at 17 000 rpm (35500*g*) for 90 min. While a pH of 8.5 was maintained by addition of 6 N NaOH, the cell-free extract was brought to 35% saturation in $(NH_4)_2SO_4$ and centrifuged in a JA-10 rotor at 10 000 rpm (13900*g*) for 60 min. The supernatant was brought to 55% saturation with $(NH_4)_2SO_4$ and centrifuged as above. The $(NH_4)_2SO_4$ pellets were resuspended in >1 L of buffer B [20 mM Tris-HCl (pH 8.5) and 10 mM β-mercaptoethanol] until the conductivity was less than 7.5 mS (Radiometer CDM83 conductivity meter). The extract was loaded onto a DEAE-Sepharose fast-flow column (4.8 × 16.5 cm) equilibrated in buffer B and washed with 750 mL of buffer B and 75 mM NaCl. The protein was eluted with a linear gradient (1.5 L of buffer B and 75 mM NaCl to 1.5 L of buffer B and 250 mM NaCl) at a flow rate of 0.5 bed volume per hour. Recombinant 3,4-PCD eluted between 150 and 190 mM NaCl. Fractions containing greater than 20% of the peak activity were pooled. The DEAE pool was brought to 1.5 M $(NH_4)_2SO_4$, centrifuged in a JA-10 rotor at 10 000 rpm (13900*g*) for 30 min, and loaded onto an octyl-Sepharose column (2.5 cm × 30.5 cm) equilibrated in buffer A and 1.5 M $(NH_4)_2SO_4$. After the mixture was washed with 300 mL buffer A and 1.5 M $(NH_4)_2SO_4$, the protein was eluted with a linear gradient [750 mL of buffer A and 1.5 M $(NH_4)_2SO_4$ to 750 mL of buffer A] at a flow rate of 0.5 bed volume per hour. Recombinant 3,4-PCD eluted between 1 and 0.6 M ammonium sulfate. The pooled octyl-Sepharose fraction was loaded onto a phenyl-Sepharose CL4B column (2.5 cm × 20 cm) equilibrated in buffer A and 0.7 M $(NH_4)_2SO_4$. After the mixture was washed with 200 mL of buffer A and 0.7 M $(NH_4)_2SO_4$, the protein was eluted with a linear gradient (500 mL of buffer A and 0.7 M $(NH_4)_2SO_4$ to 500 mL of buffer A) at a flow rate of 0.5 bed volume per hour. Recombinant 3,4-PCD eluted between 0.25 and 0.0 M ammonium sulfate. Fractions were assayed and pooled as described above. Following dialysis (12000−14000 Da molecular mass cutoff) against two changes of 4 L of buffer A, the enzyme was concentrated using an Amicon concentrator (15 psi) with a YM-100 filtration membrane. Pure, concentrated preparations were frozen in liquid nitrogen and stored at −80 °C. A typical purification is summarized in Table 1.

Table 1: Purification Summary of Recombinant 3,4-PCD[a]

step	volume (mL)	activity (U/mL)	total protein (mg)	specific activity (U/mg)	-fold purification	% yield
cell-free extract	740	13.7	18460	0.55	0	100
35% $(NH_4)_2SO_4$	800	11.6	10210	0.91	1.6	92
55% $(NH_4)_2SO_4$	1100	8.4	9780	0.94	1.7	91
DEAE-Sepharose	230	26.7	2760	2.22	4	61
octyl-Sepharose	130	38.3	360	13.8	25	49
phenyl-Sepharose	80	51.1	110	37.2	68	40

[a] Based on 300 g of wet weight cells.

Enzyme Assays and Protein Analysis. Enzymatic activity (wild-type), protein concentrations, and iron quantitation were determined as previously described (*20*). Since the mutants demonstrated extremely low activity, assays for the enzyme during purification involved SDS−PAGE (12.5% homogeneous) using a Pharmacia Phastgel system. Fractions were pooled by visual estimation of quantity and purity from standard Coomassie or silver staining procedures.

Product Identification. A quartz cuvette was filled with 987 μL of 50 mM Tris-HCl (pH 7.5) and 10 μL of enzyme (native 3,4-PCD, 0.3 mg/mL; and Y447H 3,4-PCD, 15.0 mg/mL). PCA was added to a final concentration of 100 μM for the wild-type 3,4-PCD and 180 μM for Y447H. Reactions were followed optically until no further changes were observed and are reported as difference spectra to remove the absorbance due to the enzyme.

Steady-State Kinetics. The K_M and V_{Max} were determined from a series of initial velocity measurements at increasing substrate concentrations. The constants were obtained by nonlinear regression fitting of the initial velocity data to the Michaelis−Menten equation using the program KFIT developed by N. C. Millar (Nmillar@thenet.co.uk). Reactions were carried out in 1 mL of 50 mM Tris at pH 8.5 and 25 °C using a GBC UV/visible spectrophotometer. The initial velocities were determined from linear least-squaresd regression analysis of the decrease in PCA absorption. However, since both PCA ($\epsilon = 3870$ cm^{-1} M^{-1}) and the product (β-CM, $\epsilon = 1590$ cm^{-1} M^{-1}) (*30*) absorb light at 290 nm, the observed ΔA_{290} per second was divided by the difference between the extinction coefficients ($\Delta\epsilon = 2280$ cm^{-1} M^{-1}). In assays where [O_2] was varied at several fixed PCA concentrations, the reaction buffer containing either purified native 3,4-PCD (5 μL of a 1.6 mg/mL solution) or purified

Y447H (5 μL of a 100 mg/mL solution) was equilibrated with a mixture of air and nitrogen ranging from 0.5 to 100% air. The reaction was initiated with 4 μL of 90 mM anaerobic PCA. For assays in which PCA was varied (30 μM to 6 mM) at a fixed oxygen concentration ($\sim$250 μM O_2), 5 μL of enzyme (WT, 1.6 mg/mL; and Y447H, 100 mg/mL) was used to initiate the reaction.

Dissociation Constant Measurements. Anaerobic Y447H (4.8 μM; 50 μM iron sites) in 50 mM Tris-HCl buffer (pH 8.5) was mixed with aliquots of anaerobic PCA (0.75 mM stock solution), and the optical density at 450 nm was recorded after a 10 min incubation. The fraction bound was determined as the ratio of the change in optical density relative to the maximal change after adding a large excess of PCA. This was plotted versus the free concentration of PCA and fit as a regular hyperbola using nonlinear regression analysis to yield the K_D value. The free concentration of PCA was calculated from the total concentration of PCA added, the fraction bound, and the total number of active sites present. The latter was determined by quantitative analysis of the total iron using inductively coupled plasma emission spectroscopy (Soil Sciences, University of Minnesota). Previous experiments indicate that the amount of iron present but not in active sites is very low (*20*). Dissociation constants for the wild-type recombinant enzyme were determined similarly except that the active sites concentration was 25 μM.

Spectroscopy. Optical analyses were as previously described (*20*). PCA was introduced anaerobically to anaerobic 3,4-PCD. Spectra were collected at concentrations of substrate or inhibitor which saturated the enzyme at 4 °C.

Stopped-Flow Absorption Spectroscopy Experiments. All data were collected at 25 °C as described elsewhere (*31*) using an Update Instruments stopped-flow device. Experimental parameters are given in the figure legends. Absorbance changes were monitored with either a diode array detector (Princeton Instruments) or at a single wavelength using a conventional photomultiplier detector. Pseudo-first-order conditions were established for each reaction. The data were analyzed by fitting to multiple exponential phases using nonlinear regression analysis as described previously (*31*).

Crystallization and X-ray Diffraction. Crystals of the Y447H mutant 3,4-PCD were obtained by vapor diffusion with $(NH_4)_2SO_4$ as the precipitant at 4 °C following previously reported procedures (*6*). X-ray diffraction data collection and processing were according to Orville et al. (*10*) (Table 2). Model refinement was carried out in two phases with PROTIN/PROLSQ (*32*, *33*) on a Cray YMP or C90 supercomputer. The model for the first refinement phase was derived from the wild-type 3,4-PCD structure (*6*) in which all solvent molecules in the active site were removed and Tyr447 was replaced by His. The second phase of refinement included several additional active site solvent molecules and the β-mercaptoethanol modification at $Cys429^{S\gamma}$ (*10*), as well as either (i) a solvent molecule, (ii) a SO_4^{2-} molecule, or (iii) a CO_3^{2-} molecule coordinated to the iron. There were no iron−ligand bond distance restraints during the refinements. The stereochemical quality of the final model (Table 2) was assessed with WHAT_CHECK (*34*). Figures 5 and 11 were prepared with MOLSCRIPT (*35*) and MINIMAGE/MOLSCRIPT (*36*).

Table 2: Summary of Data Collection[a] and Model Refinement

Data Collection	
resolution cutoff (Å)	2.1
*I*2 unit cell [*a*, *b*, and *c* (Å) and β (deg)]	197.4, 127.2, 134.6, 97.7
total observations (unique)	333815 (161689)
R_{merge}	0.072[b] (0.107)[c]
$R_{isomorphous}$ to native[d]	0.14
fraction of data (resolution shell)	0.78 (10−2.1 Å) 0.51 (2.2−2.1 Å)
average intensity [$I/\sigma(I)$]	7.38 (10−2.1 Å)
Model Refinement	
resolution range (Å)	6.0−2.1
reflections with $F \geq 0.01\sigma$	132596
R-factor[e]	0.18 (6.0−2.1 Å) 0.25 (2.2−2.1 Å)
rms deviation from ideal	
23 symmetry (Å)	0.18
bond distances (Å)	0.02
bond angles (deg)	3.1
number of non-hydrogen protein atoms	20502
number of solvent O atoms	1428
mean *B* values (Å^2)	
α subunit	23.7
β subunit (Fe^{3+})	16.6 (17.3)
solvent (carbonate)	18.4 (18.6)

[a] Data from one crystal. [b] Weighted $R_{merge} = [\sum_{hkl}\sum_i[(I_i - \langle I\rangle_i G_i)/\sigma_i]^2/\sum_{hkl}\sum_i(I_i/\sigma_i)^2]^{1/2}$, where, for observation *i* of reflection *hkl*, I_i is the observed intensity, $\langle I\rangle_i$ is its mean intensity, G_i is the scaling function applied, and σ_i is the standard deviation. [c] Absolute $R_{merge} = \sum_{hkl}\sum_i|I_i - \langle I\rangle_i G_i|/\sum_{hkl}\sum_i I_i$. [d] $R_{isomorphous} = \sum_{hkl}|F_{Y447H} - F_{WT}|/\sum_{hkl}F_{WT}$, where F_{Y447H} and F_{WT} are the structure factors for the 3,4-PCD as isolated from the Y447H mutant and wild-type, respectively. [e] *R*-factor $= \sum_{hkl}|F_o - F_c|/\sum_{hkl}F_c$.

RESULTS

Bacterial Cell Growth and Recombinant Enzyme Purification. In our previous study of the cloning and expression of 3,4-PCD, *Proteus mirabilis* was used as a host for expression because it contains no endogenous 3,4-PCD (*20*). However, very high levels of salicylate were required for optimal induction, leading to poor cell growth. After further study, *P. fluorescens* was identified as a strain of *Pseudomonas* reported to be lacking an endogenous 3,4-PCD (*37*), and this was subsequently verified by enzyme assay and Western analysis (see below). *P. fluorescens*, harboring expression plasmid pRWF113, has proven to be a superior host for expression, yielding higher levels of cell growth and twice the recombinant enzyme activity at lower inducer concentrations.

The α and β subunits of recombinant 3,4-PCD were apparent following PAGE and Western analysis of cell extracts from *P. fluorescens* containing pRWF158 (Figure 2). Figure 2 also demonstrates that, under a variety of growth conditions known to induce 3,4-PCD, *P. fluorescens* expresses no proteins that cross-react with 3,4-PCD polyclonal antibodies, suggesting that *P. fluorescens* contains no endogenous 3,4-PCD. Accordingly, no 3,4-PCD activity was detected under these growth conditions. 3,4-PCD was detected only in *P. fluorescens* carrying pRWF113 and induced with salicylate (Figure 2). These data show that *P. fluorescens* can be used as a host for high-level expression, purification, and characterization of recombinant 3,4 PCDs.

Purification of the recombinant wild-type enzyme as described in Experimental Procedures results in a 68-fold

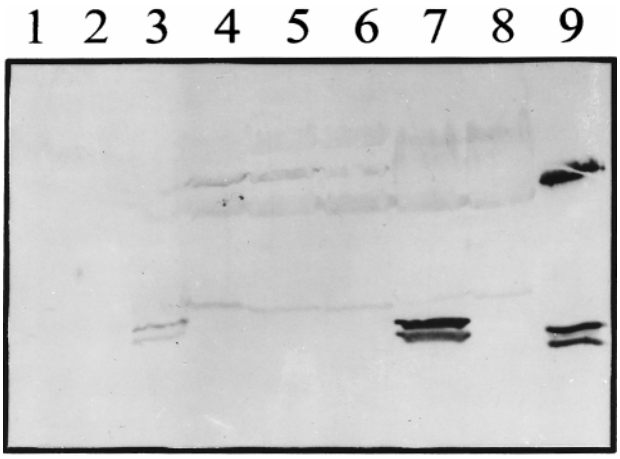

FIGURE 2: Western blot of cell-free extracts from *P. fluorescens* grown in the presence of various carbon sources under inducing and noninducing conditions for 3,4-PCD. The presence of 3,4-PCD is indicated by the two low-molecular mass bands from the similarly sized α and β subunits and the band from the $\alpha\beta$ dimer: lane 1, *P. fluorescens* grown in TB and 0.35 mM sodium salicylate; lane 2, *P. fluorescens* grown in TB; lane 3, *P. fluorescens*-pRWF113 grown in TB and 0.35 mM sodium salicylate; lane 4, *P. fluorescens*-pRWF113 grown in TB; lane 5, *P. fluorescens* grown in Hutner's minimal media and 0.5% glucose and 5 mM 4HBA; lane 6, *P. fluorescens* grown in Hutner's minimal media and 0.5% glucose; lane 7, *P. putida* (ATCC 23975) grown in Hutner's minimal media and 0.5% glucose and 5 mM 4HBA; lane 8, *P. putida* (ATCC 23975) grown in Hutner's minimal media and 0.5% glucose; and lane 9, purified natural 3,4-PCD (1 μg) from *P. putida* (ATCC 23975).

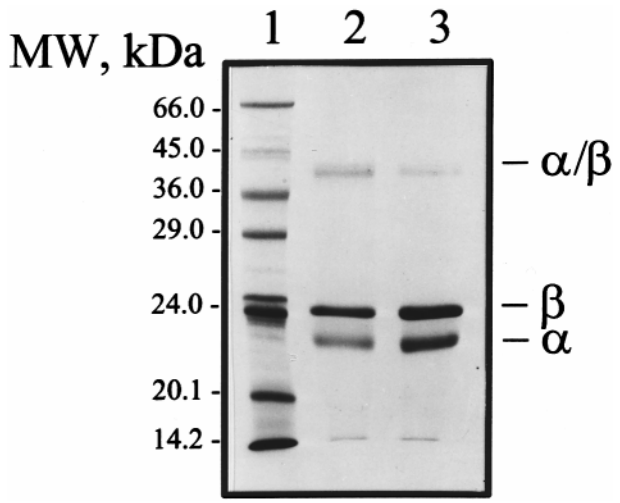

FIGURE 3: SDS−PAGE (9−18%) gel of purified Y447H and wild-type 3,4-PCD: lane 1, molecular mass markers (Sigma Inc., Dalton Mark VII-L); lane 2, Y447H (1 μg); and lane 3, purified wild-type 3,4-PCD (1 μg). The α (22 kDa) and β (25 kDa) subunits of 3,4-PCD are apparent along with a lesser amount of the $\alpha\beta$ protomer typically observed under the conditions used here.

purification and ~40% recovery (Table 1). The protocol yields apparently homogeneous preparations as shown in Figure 3. The physical and kinetic parameters of the recombinant enzyme obtained from *P. fluorescens* were essentially indistinguishable from those of the natural enzyme purified from *P. putida* (Table 3) or recombinant enzyme purified from *Pr. mirabilis* (*20*). Purification of the Y447H mutant enzyme was completed using the same protocol. Although Western analysis showed that comparable amounts of wild-type and mutant enzyme were expressed, the specific activity of the mutant enzyme was very low. This necessitated assay of column fractions by PAGE in the early stages of purification. Apparently homogeneous Y447H 3,4-PCD was obtained (Figure 3) and crystallized (see Experimental Procedures).

General Characterization. Y447H catalyzes the formation of the normal β-CM product from oxidation of PCA as revealed by its characteristic UV spectrum ($\lambda_{max} = 230$ nm, isosbestic point vs PCA spectrum, 281 nm), albeit at a greatly decreased rate relative to that of the recombinant wild-type enzyme (data not shown). No evidence for any product other than β-CM was observed. In particular, the characteristic yellow-colored products of ring cleavage outside the vicinal hydroxyl groups were not observed, showing that the fundamental catalytic specificity of the wild-type enzyme is maintained. The enzyme activity of Y447H was monitored both by O_2 uptake using an oxygen electrode (*38*) and by the rate of decrease of the characteristic 290 nm optical maximum of PCA. Both assay methods gave the same specific activity and the same absolute utilization of the two substrates, showing that the mutation does not uncouple the strictly stoichiometric O_2 utilization and substrate oxidation characteristic of this enzyme class.

The kinetic parameters for wild-type and recombinant 3,4-PCD are compared with those of Y447H in Table 3. The wild-type and recombinant enzymes are comparable in their values of K_M for PCA and O_2, as well as in their k_{cat} values (proportional to V_{Max}). In contrast, the Y447H mutant exhibited a 10-fold lower $K_{M\ PCA}$ value and an approximately 600-fold lower k_{cat} at 25 °C. The k_{cat} calculation is based on the number of iron-containing active sites present in the enzyme. For the wild-type enzyme, there are less than 12 functional active sites per holoenzyme as observed in the crystal structure because only about half bind Fe^{3+} (*39*). In contrast, Fe^{3+} is bound in greater than 80% of the active sites of the purified Y447H mutant holoenzyme. The ratio of k_{cat} to $K_{M\ PCA}$ provides a measure of the efficiency of the enzyme. The wild-type and recombinant enzymes have a $k_{cat}/K_{M\ PCA}$ within approximately 2 orders of magnitude of the diffusion-controlled limit, whereas the mutant is 45−50-fold less efficient. The Y447H K_M for O_2 is too low to be determined directly by our methods, but it is certainly lower than 6 μM as indicated in Table 3. Thus, it is likely that the K_M for O_2 is also at least 10-fold lower than that observed for the wild-type enzyme.

Optical Spectrum of the Y447H Mutant. The optical spectrum of the Y447H mutant enzyme shown in Figure 4 (solid line) is bleached in the 460−700 nm region relative to that of the wild-type enzyme (dotted line) (*39*). The spectrum of the yellow mutant enzyme exhibits spectral shoulders at 410 and about 690 nm. The bleached spectrum in the 460−700 nm range is expected on the basis of the loss of one tyrosine from the iron ligation sphere.

Structure of the Y447H Mutant. The Y447H mutant 3,4-PCD crystallized isomorphously to the wild-type enzyme. Analysis of the structural data shows that there are no significant differences between the wild-type and the Y447H mutant 3,4-PCD outside the active site. The initial averaged $(|F_{Y447H}| - |F_{WT}|)e^{-i\alpha(WT)}$ Fourier maps contoured at $\pm 5\sigma$ for the Y447H mutant active site region are shown in Figure 5a superimposed on the structure of the native enzyme. The largest negative feature in the map is a consequence of the

Table 3: Comparison of Physical and Kinetic Properties[a]

enzyme	$K_{D\ PCA}$ (μM)	$K_{M\ PCA}$ (μM)	$K_{M\ oxygen}$ (μM)	k_{cat}[b] (s^{-1})	$k_{cat}/K_{M\ PCA}$ ($\times 10^6\ M^{-1}\ s^{-1}$)	mol of Fe^{3+}/ mol of PCD
natural 3,4-PCD[c]	10	30	40	70	2.33	6
recombinant WT	10	29	56	68	2.34	6.5
mutant Y447H	40	2.9	<6[d]	0.12	0.05	10.5

[a] At 25 °C. [b] Normalized to the number of active sites that contain Fe^{3+}. [c] Adapted from ref *1*. [d] Maximal velocity did not change significantly from 250 to 20 μM oxygen, suggesting $K_M < 6\ \mu$M.

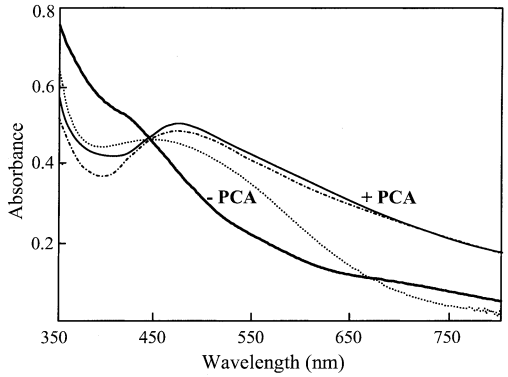

FIGURE 4: Comparison of the optical absorption spectra of Y447H and wild-type 3,4-PCD. The enzyme and complexes were prepared in 50 mM Tris-HCl at pH 8.5 under anaerobic conditions: Y447H (145 μM Fe^{3+} sites) as isolated (heavy solid line) and plus 1 mM PCA (light solid line) and wild-type enzyme (145 μM Fe^{3+} sites) as isolated (dotted line) and plus 1 mM PCA (dashed−dotted line).

Tyr447 to His447 mutation and clearly suggests that, in contrast to Tyr447, His447 does not coordinate the iron. In addition, the bound hydroxide molecule, Wat827, has either dissociated or shifted to a new coordination site on the Fe^{3+}. The locations of the five coplanar solvent molecules normally found within the active site cavity have also been shifted.

After the first phase of refinement (see Experimental Procedures), a large positive feature in the $|F_o| - |F_c|$ electron density maps clearly indicated the presence of an exogenous ligand to the active site iron (not shown). The peak intensity of this difference feature in the average difference map was approximately 20σ. In contrast, the peak difference intensity typical of solvent molecules in the active site, but remote from the iron, was between 4 and 8σ. A solvent molecule was placed into each of these difference features in the active site as well as the 20σ peak adjacent to the iron. Two additional models were also independently refined, each with either a SO_4^{2-} or a CO_3^{2-} molecule placed into the 20σ difference density rather than the solvent molecule. Each model was refined to equivalent *R*-factors, but the averaged $2|F_o| - |F_c|$ and $|F_o| - |F_c|$ electron density maps as well as the occupancy and thermal factors for the CO_3^{2-} model were far superior to either the SO_4^{2-} or solvent model. The final $2|F_o| - |F_c|$ electron density map superimposed on the carbonate model is shown in Figure 5b. This structural analysis suggests that carbonate (or bicarbonate), apparently originating from atmospheric CO_2, coordinates the iron in the Y447H mutant 3,4-PCD.

The bond distances and bond angles for the iron coordination sphere are compared to those of the wild-type 3,4-PCD·PCA complex in Table 4. A comparison of the Y447H mutant 3,4-PCD structure to that of the uncomplexed and anaerobic PCA complex of the wild-type enzyme is shown in Figure 5c. From these comparisons, it is clear that the putative carbonate anion asymmetrically chelates the iron in a manner similar to that observed for PCA in the anaerobic 3,4-PCD·PCA complex of the wild-type enzyme. The short $Fe^{3+}-carbonate^{O1}$ bond is trans to $His462^{N\epsilon 2}$, whereas the longer $Fe^{3+}-carbonate^{O2}$ bond is trans to $Tyr408^{O\eta}$. This is similar to the distortion in the $PCA\cdot Fe^{3+}$ chelate complex of the wild-type enzyme (*7*); however, the resulting asymmetry of the carbonate chelate is more extreme than that in the PCA complex. The bond distances and bond angles suggest that the axial ligand axis of the trigonal bipyramidal coordination sphere is aligned with the $Tyr408^{O\eta}$ and $carbonate^{O2}$ ligands.

Electrostatic neutrality on the ferric ion in the Y447H mutant is maintained by assuming that the bound form is CO_3^{2-}. This is also consistent with the presumption that the large positive electrostatic potential adjacent to the iron, due in large part to the guanidinium group of Arg457, would disfavor additional positive electrostatic potential on the metal center. Hydrogen bonding to the axial and equatorial oxygen atoms of the carbonate appears to stabilize the iron in the active site relative to the wild type. Indeed, the thermal factors for the iron in the mutant (17 Å^2) are 2-fold lower than those in the wild-type structure (34 Å^2) (*6*). This may also corroborate the observation of greater iron incorporation in this mutant relative to that in wild-type 3,4-PCD based upon elemental analysis.

The structure of the polypeptide backbone around the mutation site is essentially unaltered relative to the wild-type structure. Because His residues are shorter than the Tyr residues, His447 cannot coordinate the iron, and consequently, $His447^{N\epsilon 2}$ and $His447^{N\delta 1}$ participate in hydrogen bonding with $carbonate^{O1}$ and $Pro448^{O}$, respectively (Figure 5c). These interactions suggest a positive charge on His447 and stabilize the side chain in an orientation between the positions of Tyr447 in the uncomplexed and anaerobic PCA complex, respectively, of the wild-type 3,4-PCD (Figure 5c). The carbonate O1 atom is 1.8 Å from the Fe^{3+}, forms a 108° $His460^{N\epsilon 2}-Fe^{3+}-carbonate^{O1}$ bond angle, and forms a 3.0 Å hydrogen bond with $His447^{N\epsilon 2}$. In the wild-type enzyme, the distance between the position of $Tyr447^{O\eta}$ in the uncomplexed structure and that of PCA^{O4} in the substrate complex is only 0.9 Å, and consequently, Tyr447 must rotate out of the way upon substrate binding. In the wild-type substrate complex, PCA^{O4} is 2.2 Å from the iron and forms a 101° $His460^{N\epsilon 2}-Fe^{3+}-PCA^{O4}$ bond angle. In the Y447H mutant, the Fe^{3+} atom is displaced approximately 0.6 Å relative to its position in the native 3,4-PCD·PCA structure, and the distance between the position of $His447^{N\epsilon 2}$ and the position of PCA^{O4} in the substrate complex structure is 2.6 Å. On the basis of these measurements, there is no compelling structural reason that substrate binding to the mutant enzyme would require His447 to rotate

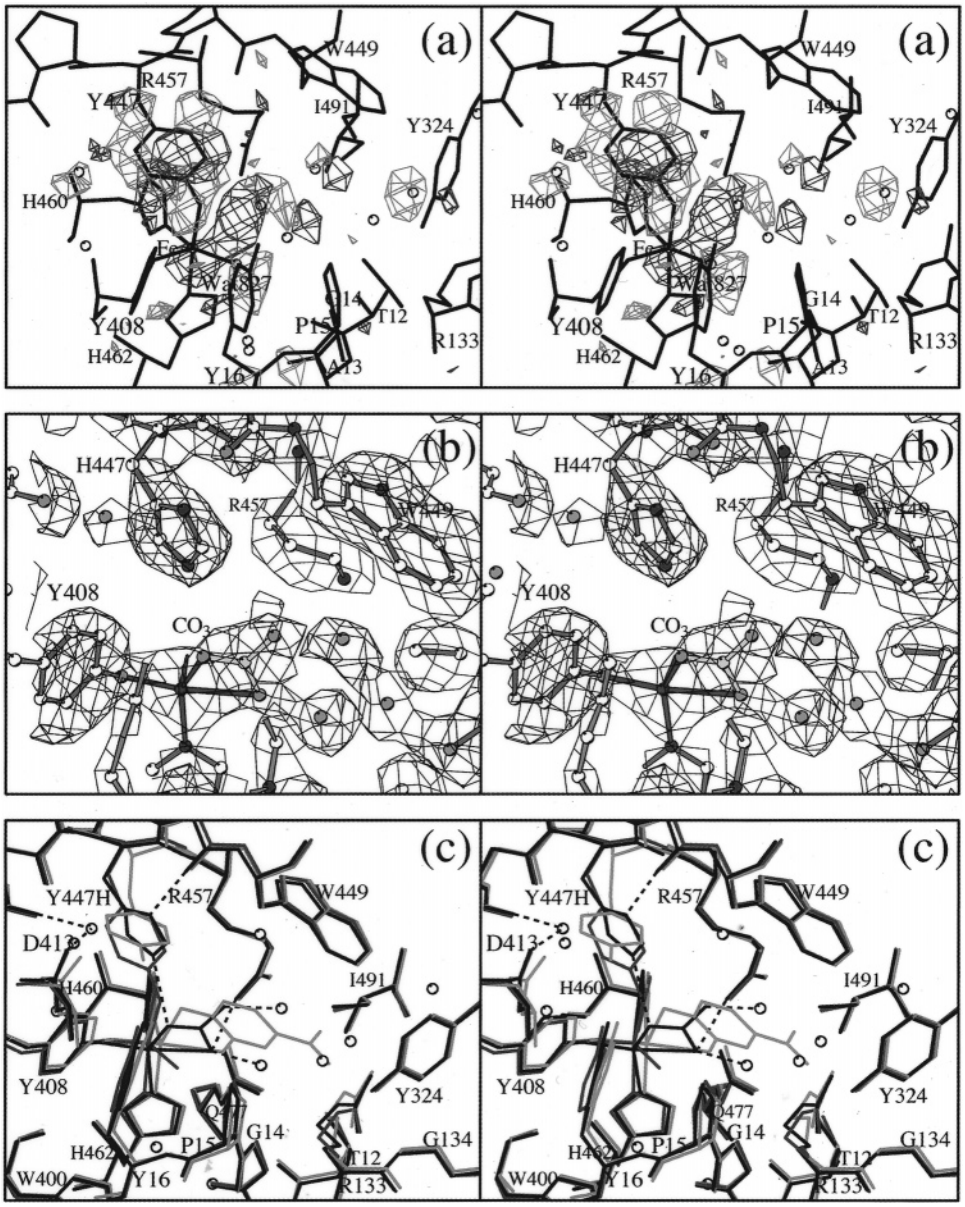

FIGURE 5: Divergent stereoviews of the structure and electron density maps for the Y447H mutant 3,4-PCD. (a) The initial averaged difference Fourier maps contoured at $\pm 5\sigma$ superimposed on the wild-type 3,4-PCD uncomplexed structure. Maps of the form $(|F_{Y447H}| - |F_{WT}|)e^{-i\alpha(WT)}$ were calculated with structure factors from the mutant and wild type, respectively, using calculated phases from the refined wild-type structure. Positive difference contour levels are blue, whereas negative levels are red. (b) The final averaged $2|F_o| - |F_c|$ electron density maps contoured at 1σ for the Y447H 3,4-PCD·CO_3 model. (c) Comparison of the Y447H 3,4-PCD·CO_3 model (black lines; dashed lines indicate hydrogen bonds), the wild-type uncomplexed structure (blue lines), and the wild-type 3,4-PCD·PCA complex (red lines).

into an orientation analogous to that observed for Tyr447 in the wild-type substrate complex.[4] On the other hand, if His447 does change orientation upon PCA binding, then His447$^{N\delta1}$ could hydrogen bond with Gly406^{O}. From this orientation, His447$^{N\epsilon2}$ would be too far away to form hydrogen bonds with Tyr16^{OH} and Asp413$^{O\delta1}$ analogous to those formed by Tyr447^{OH} in the wild-type structures.

Substrate Complex of Y447H. The anaerobic addition of PCA to Y447H causes a discrete maximum to form at 485 nm in the optical spectrum (Figure 4). In addition, a large increase in extinction is noted in the 440−800 nm region. An essentially identical spectrum is observed for the substrate complex of the wild-type enzyme (see Figure 4) (*39*). The red shift of the maximum and the increase in long-wavelength absorbance have been attributed to the formation of two new iron−catecholate bonds as substrate chelates the iron (*4*, *9*, *11*). It is probably also due, in part, to the loss of a bond from the Tyr447. Thus, the substrate complex for Y447H appears to involve direct coordination of the substrate to the iron, probably as a chelate complex very similar to that observed for the wild-type enzyme.[4]

The changes in the optical spectrum that occur as substrate binds allow the determination of a dissociation constant for the complex. K_D values of 10 and 40 μM (each $\pm$20%) were determined for the recombinant wild-type enzyme and Y447H, respectively, in 50 mM Tris-HCl at pH 7.5 and 25 °C (Table 3).

[4] N. Elango, K. B. Dolbeare, J. D. Lipscomb, and D. H. Ohlendorf, unpublished observations. The preliminary structure of a substrate−analogue complex of Y447H shows that the analogue chelates the iron, the carbonate is displaced, and His447 remains approximately in the same location.

Table 4: Distances[a] and Angles[b] for the Active Site Fe^{3+}

	Y447H	WT PCA complex[c]
distance (Å)		
$Tyr408^{O\eta}$−Fe	1.9	2.0
$His460^{N\epsilon2}$−Fe	2.3	2.3
$His462^{N\epsilon2}$−Fe	2.1	2.2
$carbonate^{O2}$−Fe	2.5	2.4 (PCA^{O3})
$carbonate^{O1}$−Fe	1.8	2.2 (PCA^{O4})
$His447^{N\epsilon2}$−Fe	4.3	7.7 ($Tyr447^{OH}$)
angle (deg)		
$Tyr408^{O\eta}$−Fe−$His460^{N\epsilon2}$	89	90
$Tyr408^{O\eta}$−Fe−$His462^{N\epsilon2}$	105	96
$Tyr408^{O\eta}$−Fe−$carbonate^{O2}$	168	171 (PCA^{O3})
$Tyr408^{O\eta}$−Fe−$carbonate^{O1}$	106	103 (PCA^{O4})
$His460^{N\epsilon2}$−Fe−$His462^{N\epsilon2}$	91	92
$His460^{N\epsilon2}$−Fe−$carbonate^{O2}$	95	99 (PCA^{O3})
$His460^{N\epsilon2}$−Fe−$carbonate^{O1}$	108	101 (PCA^{O4})
$His462^{N\epsilon2}$−Fe−$carbonate^{O2}$	87	85 (PCA^{O3})
$His462^{N\epsilon2}$−Fe−$carbonate^{O1}$	145	157 (PCA^{O4})
$carbonate^{O1}$−Fe−$carbonate^{O2}$	63	75 (PCA^{O3} and PCA^{O4})

[a] Estimated bond distance errors are ~0.25 Å on the basis of Luzzati (*42*) analysis. [b] Estimated bond angle errors are ±3°. [c] The wild-type 3,4-PCD·PCA complex (*7*).

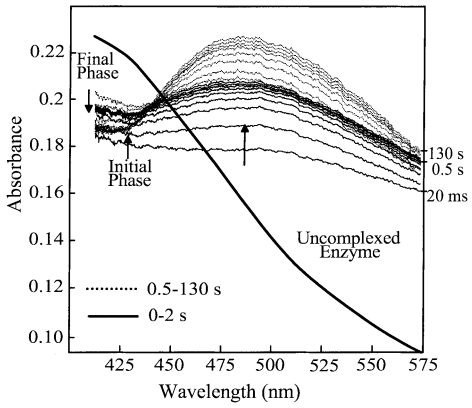

FIGURE 6: Rapid scan stopped-flow optical spectra of the binding of PCA to Y447H mutant 3,4-PCD. Anaerobic Y447H (130 μM Fe^{3+} sites) in 50 mM Tris-HCl at pH 8.5 was mixed 1:1 with anaerobic 4 mM PCA in the same buffer at 25 °C using a stopped-flow device. The reaction time course was monitored using a diode array detector at 20 ms intervals, and then a second identical reaction was monitored at 500 ms intervals. Every 10th spectrum is shown for each time domain (see the legend on the figure) for clarity. The spectrum of the uncomplexed Y447H at the concentration of the enzyme after mixing is shown as a heavy solid line for reference.

Transient Kinetics of Substrate Binding. PCA binding to wild-type 3,4-PCD occurs at a rate that is at the high limit for determination by stopped-flow techniques (*40*, *41*). However, estimates of the rate from the two independent studies cited suggest that it occurs with a rate constant in excess of 2×10^6 M^{-1} s^{-1} at 4 °C. In contrast, the rate of PCA binding to Y447H 3,4-PCD is readily followed using a stopped-flow device and a rapid scan diode array detector as shown in Figure 6. It is evident that the binding process proceeds through at least two intermediates. The final step of the reaction proceeds relatively slowly, and the spectra exhibit an isosbestic point at 430 nm suggesting that only two forms of the enzyme exist in this phase. However, the initial step(s) of the reaction does not exhibit such an isosbestic point, so other, more rapidly formed intermediates must precede the final step of the reaction. Analysis of the reaction time course by selecting time slices at specific wavelengths from the diode array data or using a single-wavelength detector (which allows more rapid data collection) shows that the reaction actually has several intermediates (Figure 7). Followed at 525 nm under pseudo-first-order conditions (large excess of PCA) at 25 °C, the reaction time course was best fit as the sum of three exponential phases with observed reciprocal relaxation times (rate constants for irreversible reactions) of 3.5 ± 0.5, 0.6 ± 0.15, and 0.09 ± 0.02 s^{-1}. The same reciprocal relaxation times within experimental error were obtained when the optical change was followed at 400 nm, but the final two phases were observed to proceed with decreasing absorbance. An attempt was made to fit the 400 nm data with only two exponential phases, but an adequate fit could not be obtained (Figure 7B, dashed line). When the PCA concentration was varied in the range of 0.5−5.0 mM, no changes in the observed rate constants were apparent for any phase at either wavelength (data not shown). This would not be the case if the actual second-order binding step was observed or if the binding step was reversibly connected to the observed steps. This suggests that there is an unobserved step in which substrate binds in the active site ahead of the observed steps. This step must be either irreversible [$K_{D\,1}$ (see below) approaches zero] or in rapid equilibrium compared to the other steps and saturated ($K_{D\,1} \ll$ [PCA]), making it effectively irreversible. The first observed phase of the reaction begins with an optical density significantly less than that of the resting enzyme at 400 nm, suggesting that the spectrum is bleached in this initial fast phase, but our methods are not fast enough to determine the spectrum of

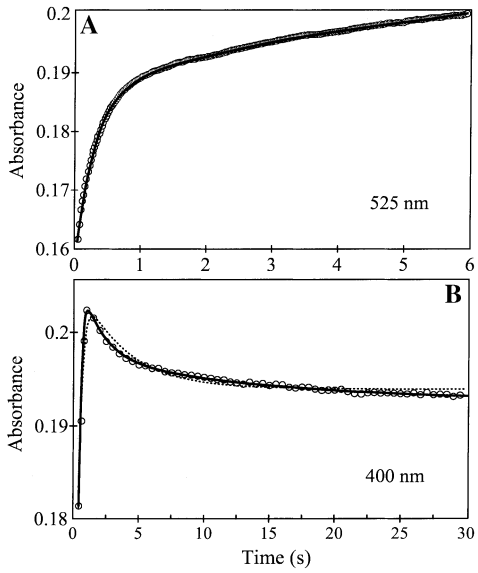

FIGURE 7: Time course of PCA binding to Y447H. Single-wavelength time course data were extracted from data sets analogous to those shown in Figure 6 (open circles) and fitted to summed exponentials using nonlinear regression (solid lines). (A) Time course recorded at 525 nm recorded at 20 ms intervals and fitted to three summed exponentials (reciprocal relaxation times of 3.5 ± 0.5, 0.6 ± 0.15, and 0.09 ± 0.02 s^{-1}). (B) Time course recorded at 400 nm at 0.2 s intervals (first 1 s) and then 0.5 s intervals (1−30 s) and fit to three summed exponentials. The fastest exponential was assigned a reciprocal relaxation time of 3.5 s^{-1} because there were insufficient data to determine an accurate fit. Data recorded at 20 ms intervals at this wavelength are fit well using a 3.5 s^{-1} reciprocal relaxation time (data not shown). The reciprocal relaxation times for the second two exponentials were determined to be 0.6 ± 0.05 and 0.085 ± 0.01 s^{-1}. The dashed line in panel B is the two-exponential fit for the data.

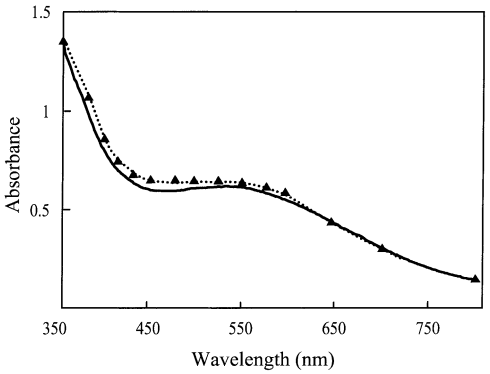

FIGURE 8: Comparison of the optical spectra of the ESO_2* intermediates of Y447H and wild-type 3,4-PCD. (Solid line) Anaerobic Y447H (600 μM Fe^{3+} sites) in 50 mM Tris-HCl (pH 8.5) and 4 mM PCA was mixed 1:1 at 4 °C with the same buffer saturated with pure O_2 (equilibrated at 25 °C, ~1.4 mM) using a stopped-flow device. Spectra were recorded using a diode array detector at 20 ms intervals. The spectrum shown is the first spectrum obtained and represents the average of 15 experiments. (Dotted line) The spectrum of the same intermediate from the wild-type enzyme isolated from *Pseudomonas cepacia* reconstructed from a series of single-wavelength measurements (triangles) (*41*) is shown superimposed and scaled to the spectrum from the Y447H intermediate for reference. The intermediate from 3,4-PCD isolated from *P. cepacia* has spectral features very similar to those of the intermediate observed for the wild-type enzyme from *P. putida* used here (*40*, *41*).

this first intermediate. The transient kinetic evaluation of anaerobic substrate binding thus suggests that the process must have at least four steps. The simplest (but not unique) interpretation is

$$E \overset{K_{D\,1}}{\rightleftharpoons} ES_1 \rightleftharpoons ES_2 \rightleftharpoons ES_3 \rightleftharpoons ES_4$$

Spectra of Y447H·PCA·O_2 Complexes. Rapid mixing of an anaerobic, preformed 1:1 complex of Y447H·PCA with buffer containing excess O_2 allowed a single turnover to occur. The concentrations of Y447H and PCA used were well above the $K_{D\,PCA}$ so that the complex was nearly completely formed at the start of the reaction. The formation of a new intermediate was complete before the first spectrum was recorded at 20 ms (Figure 8, solid line). The spectrum of the intermediate is essentially identical with that formed by wild-type enzyme reacted in the same manner (Figure 8, dotted line). This intermediate, termed ESO_2*, is believed to be the product complex of the enzyme (*40*). In the reaction cycle of the wild-type enzyme, ESO_2* decays very rapidly (k = 36 s^{-1} at 4 °C) to the resting enzyme or the substrate complex depending upon whether excess substrate is present. The decay of the intermediate for Y447H is much slower and passes through another intermediate that has a spectrum similar to, but easily distinguishable from, that of the substrate-free enzyme (Figure 9). This new intermediate (ESO_2**) then decays to the substrate-free enzyme while exhibiting an isosbestic point at about 525 nm. These data indicate that the decay of the enzyme−substrate complex upon reaction with O_2 must consist of at least three steps, the simplest form of which is given by

$$ES_4 + O_2 \rightleftharpoons ESO_2^* \rightleftharpoons ESO_2^{**} \rightarrow E$$

The last step is likely to be irreversible because the spectrum

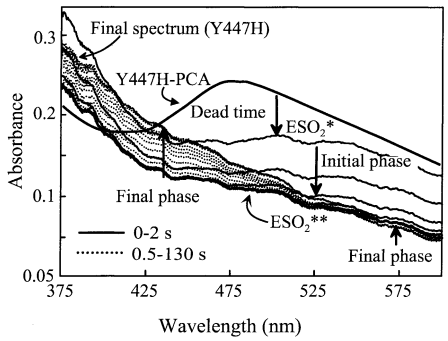

FIGURE 9: Rapid scan stopped-flow optical spectra of the reaction of O_2 with the Y447H·PCA complex. Anaerobic Y447H (130 μM Fe^{3+} sites) in 50 mM Tris-HCl (pH 8.5) and 130 μM PCA was mixed 1:1 with the same buffer saturated with pure O_2 (~1.4 mM) at 25 °C using a stopped-flow device. The reaction time course was monitored using a diode array detector at 20 ms intervals, and then a second identical reaction was monitored at 500 ms intervals. Every 10th spectrum is shown for each time domain for clarity (see the legend on the figure). The spectrum of the final Y447H·PCA complex (ES_4) at the concentration of the enzyme after mixing is shown as a heavy solid line for reference. The premixed Y447H·PCA complex was assumed to be saturated, and the 1:1 mixture limited the turnover to a single cycle ending with uncomplexed Y447H mutant 3,4-PCD.

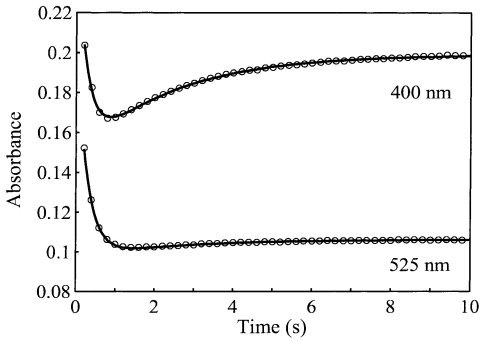

FIGURE 10: Time course of product formation upon O_2 reaction with a premixed Y447H·PCA complex. Single-wavelength time course data were extracted from an experiment conducted under the same conditions described in Figure 9 except that the spectra were recorded at 200 ms intervals (open circles) and fitted to two summed exponentials using nonlinear regression (solid line). (Top) Time course recorded at 400 nm (reciprocal relaxation times of 3.5 ± 0.3 and 0.43 ± 0.05 s^{-1}). (Bottom) Time course at 525 nm (reciprocal relaxation times of 3.5 ± 0.3 and 0.4 ± 0.15 s^{-1}). The last phase of this time course has a very low amplitude because the data were recorded at a wavelength close to the isosbestic point for the ESO_2** to uncomplexed Y447H conversion.

of the resting, substrate-free enzyme is restored. The conversion of ES_4 to ESO_2* is fast and probably passes through an ESO_2 intermediate (perhaps an organic peroxy intermediate) as reported for the native enzyme (*41*), but this has thus far not been observed. Reciprocal relaxation times of 3.5 ± 0.3 and 0.43 ± 0.05 s^{-1} were determined for the decay for ESO_2* and ESO_2**, respectively, from two exponential fits of single-wavelength data as shown in Figure 10. The major change in this conversion is an increase in extinction in the spectral range of <410 nm. The ESO_2** species is unlike any observed for the wild-type enzyme during turnover, and its possible significance will be discussed below.

DISCUSSION

The replacement of Tyr447 in 3,4-PCD by histidine has been shown here to profoundly affect the spectroscopic and

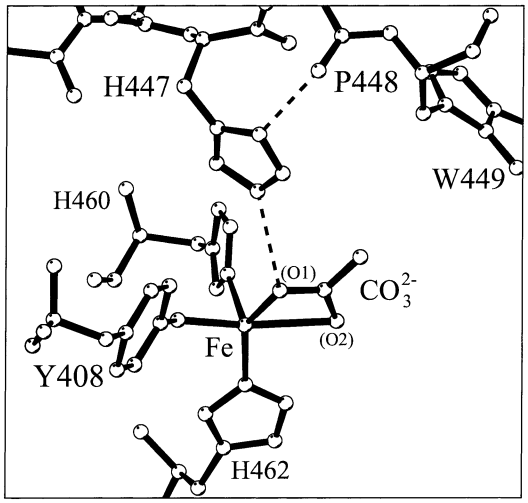

FIGURE 11: Iron coordination environment in the crystal structure of the Y447H mutant 3,4-PCD. The dashed lines represent the $H447^{N\epsilon 2}$ to carbonate and $H447^{N\delta 1}$ to $P448^{O}$ hydrogen bonds.

kinetic features of the enzyme. However, neither the nature nor the specificity of the ring cleavage reaction is altered by the mutation, and the known intermediates in the reaction cycle of the wild-type enzyme can be recognized in the reaction cycle of the mutant. Consequently, it is likely that the substrate binding and oxygen activation and insertion reactions are fundamentally unchanged. The observation that some parts of the reaction cycle are greatly decreased in rate is useful in two ways. First, it allows the specific steps which are most affected by Tyr447 to be identified, and second, it allows intermediates to be detected in these steps that are not apparent in the equivalent reactions of the wild-type enzyme. In the following discussion, we relate the intermediates that have been detected to those that are proposed to exist.

Structure. The structural aspects of the active site of Y447H are summarized in Figure 11 and Table 4. Since the changes in structure from the native enzyme appear to be localized to rather subtle changes in this region, Y447H appears to be a good system in which to investigate the effect of changes in the iron site environment on catalysis. Histidine was chosen for the substitution because it can potentially become a good Fe^{3+} ligand and might substitute for Tyr in its proposed role as an active site base. Although His is about 2 Å shorter than Tyr, comparisons with the local structure of the vestigial active site located in the α subunit of 3,4-PCD (*6*) suggested that there might be sufficient flexibility in the antiparallel β sheet containing residue 447 to allow a His in this position to coordinate to the iron. This turned out not to be the case, and the new histidine is stabilized in a position off the iron roughly midway between the two orientations for Tyr447 in the native enzyme with and without substrate bound, respectively. In this position, His447 would not interfere sterically with substrate binding, based on structural comparisons with the native enzyme substrate complex. Despite the fact that His447 does not bind to the iron, it has significant effects on catalysis and engenders some changes in active site structure.

The most dramatic new feature of the Y447H structure is the likely presence of a carbonate (or bicarbonate) as a new iron ligand. In retrospect, this is a logical ligand for the Fe^{3+} in Y447H because it takes advantage of the fact that

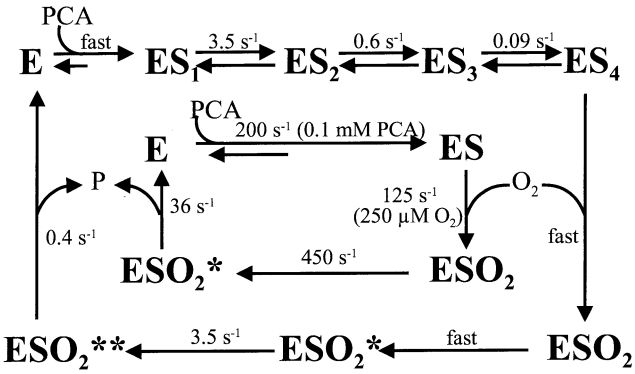

FIGURE 12: Comparison of the rates of interconversion of intermediates detected in the reaction cycles of Y447H mutant 3,4-PCD (outer cycle) at 25 °C and wild-type 3,4-PCD (inner cycle) at 4 °C (compiled from refs *40* and *41*). The two cycles are independent, and there is no interconversion of the intermediates. The cycles are drawn together only to facilitate comparison.

two vicinal iron sites are available in the mutant that can be occupied by exogenous ligands and serves to maintain the pentacoordinate ligation of the native structure through addition of only one ligand. Moreover, the addition of two negative charges upon carbonate binding would restore a neutral metal center which is observed for native and all ligand complexes of 3,4-PCD that have been structurally characterized (*7*, *10*, *11*). The fact that Wat827 is OH^- in the native enzyme and apparently CO_3^{2-} in the mutant underscores the tendency of the metal center to maintain neutrality, which we believe has important mechanistic significance as discussed below. It is interesting to point out that the structure of the probable CO_3^{2-}−iron complex observed for Y447H is strikingly analogous to that of the ferric center of the transferrins (*43*, *44*). Indeed, the bicarbonate in the transferrin structures also binds in an asymmetric manner, and there is hydrogen bonding to a nearby Arg residue.

Thus far, attempts to demonstrate that bicarbonate is an inhibitor for either native 3,4-PCD or Y447H have not been successful. If the carbonate dissociation occurs early in the substrate binding sequence, then the results presented here indicate that this process would not be rate-limiting, and thus not perturb the steady-state kinetic parameters.

Intermediates. The rates for interconversion of intermediates and comparison to the reported interconversion rates for the native enzyme are shown in Figure 12. The binding of PCA, and alternate substrates such as 3,4-dihydroxyphenyl acetate that have lower turnover numbers, are comparatively fast processes. To the extent that they can be evaluated by transient kinetic techniques, they are described well as a reversible second-order association processes (*40*, *41*). Some indication that substrate binding is, in fact, more complex was derived from our study of the binding of the strong substrate analogue inhibitors isonicotinic acid *N*-oxide (INO) and nicotinic acid *N*-oxide (NNO) (*45*). Crystal structures of these inhibitor complexes with 3,4-PCD (*7*) show that they bind in the same position as PCA and cause dissociation of Tyr447, but they are not turned over by the enzyme. Despite the fact that these inhibitors form very strong complexes with the enzyme, their binding reactions are slow and have at least three intermediates that differ significantly in their spectral properties. A similar series of intermediates is observed here, but the spectral properties of the intermedi-

ates are different. Most significantly, the final species in the INO and NNO binding processes is bleached and associated with binding of the ketonized tautomer of these inhibitors, while the final intermediate observed here is dark blue and likely to be the dianionic PCA complex on the basis of an analogy to model complexes. The spectrum of one of the transient intermediates in the binding of the *N*-oxides is also optically similar to that of the dianionic substrate complex of the mutant, suggesting that these inhibitors pass through this state before assuming the stable ketonized tautomeric form.

The existence of a series of steps in the substrate binding process was predicted from structural studies of a series of aromatic inhibitors and substrate complexes of the enzyme as described in the introductory section (*7*, *10*). Depending on the size and nature of the ring substituents, different orientations for the binding molecule were observed in the active site. Due to structural constraints within the active site of the resting enzyme revealed by the crystal structure, the predicted early intermediates would be relatively weakly associated with the iron, forming either no direct bond or a monodentate bond through the C4-O^- function. This bond would form opposite Tyr408$^{O\eta}$ which would further weaken it due to the influence of the negative *trans* ligand. As a result, a comparatively less intense and shifted LMCT band would be expected for these early intermediates relative to that of the final chelated E·PCA complex in which a strong second Fe^{3+}·PCA^{O^-} bond forms. This is what is found for each of the intermediates that are actually observed. After an initial bleaching relative to the resting Y447H enzyme, each intermediate becomes more intense and shifts toward the final maximum absorbance wavelength. Thus, the series of intermediates we observe is consistent with the stepwise progression of enzyme−substrate complexes previously proposed.

The rates of interconversion of the intermediates in the substrate binding process become progressively slower with the formation of the final ES_4 complex representing the rate-limiting step in both substrate binding and turnover. This is consistent with a linear progression of steps, but it does not rule out parallel or reversible dead-end steps leading eventually to the ES_4 complex. Moreover, the likely presence of carbonate in the iron coordination may perturb both the binding kinetics and the optical spectral changes that are observed. For example, the large decrease in absorbance during the first, very fast phase of substrate binding to Y447H is unexpected because the progressive substrate association model would predict that only minor orientation changes in the iron ligands should occur at this stage. One possibility is that the binding of the putative carbonate is perturbed in this step, ultimately leading to carbonate displacement in this or the following step, due to the steric bulk of the substrate binding in the active site.[5] Loss of a negatively charged carbonate opposite Tyr408 would facilitate charge transfer to the iron from the latter ligand and shift the observed optical spectrum to the red, thus causing a bleaching in the 450 nm region as observed. These questions can be investigated through the study of the binding of other substrates and through systematic variation of dissolved CO_2 concentrations and other reaction conditions; these studies are in progress.

The optical data presented here strongly indicate that the substrate binding processes of native and Y447H enzymes conclude with very similar enzyme−substrate complexes.[4] This is in accord with the crystallographic studies of the static enzyme·PCA complex which showed that Tyr447 is dissociated when substrate binds, and thus, it should not contribute to the optical properties of the iron in this complex (*7*). If this dissociation also occurs during catalysis, Tyr447 would not be expected to influence the chemistry of subsequent steps directly through its role as a metal ligand. Accordingly, as observed for the native enzyme, the reaction of the Y447H·PCA complex with O_2 is very fast. Our current results indicate that, to a first approximation, the chemical steps of the cycle appear to proceed with similar efficiency in the mutated and native enzymes which is consistent with the dissociation of the Tyr during these steps in the native enzyme cycle.

It is interesting to note that Y447H has a lower K_M value for O_2 than the native enzyme. One possible explanation for this would be an increase in the rate of O_2 binding. On the basis of the crystal structure of the wild-type E·PCA and E·INO·CN complexes (*7*), we have proposed that the release of Tyr447 from the iron has an effect beyond the provision of an appropriately placed active site base. It also appears to allow formation of a solvent-excluded pocket the size of O_2 immediately adjacent to the site of substrate ring cleavage. In this way, the enzyme controls the order of PCA and O_2 binding as well as directing the site of O_2 attack on the substrate. Our preliminary crystal structure of the Y447H substrate analogue complex[4] suggests that the O_2 cavity is more accessible than that in the wild-type substrate complex. Thus, the smaller size and location of His447 may facilitate O_2 entry and consequently affect the observed K_M value.

The optical spectrum of the ESO_2* product complex is readily detected using slow alternative substrates of 3,4-PCD because the decrease in rate for these substrates can be attributed to slow product release (*40*). ESO_2* formed with PCA as the substrate is much less stable, but its spectrum has been reconstructed from separate transient kinetics experiments at different wavelengths (*41*). The spectrum is red-shifted relative to those formed by the slower substrates, but it is superimposable on that of the ESO_2* formed by reacting ES_4 of Y447H with O_2 (Figure 8). This is again consistent with the reaction being largely unaffected by the mutation during the product-forming steps in which the Tyr447 is thought to be off the iron. However, in the case of Y447H, the dissociation of the PCA product is slow and apparently passes through intermediate ESO_2** which has not been previously observed. One interpretation of these observations is that a major role of Tyr447 and the solvent OH^- ligands is to serve as appropriately placed active site bases which facilitate deprotonation of PCA as it binds to the iron (*1*, *9*). Similarly, these groups may subsequently serve to promote protonation of the anionic product at the end of the reaction so that it can leave the positive region of the active site near the iron. Although carbonate and His447 might act as active site bases, they are poorly matched to

[5] Preliminary studies show that the absolute amplitudes of the fast unobserved and first observed phases are significantly increased by the presence of sodium bicarbonate in the reaction solution while subsequent phases are unaffected (K. B. Dolbeare and J. D. Lipscomb, unpublished observations). This is consistent with our hypothesis that carbonate dissociation occurs during the initial phases of the reaction.

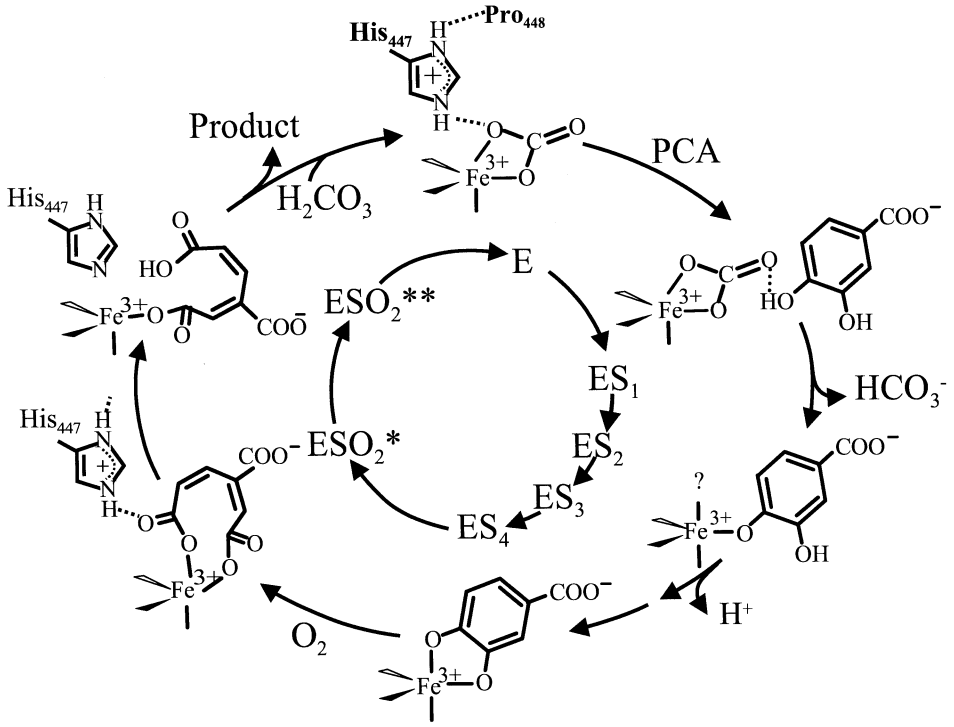

FIGURE 13: Proposed reaction cycle for Y447H mutant 3,4-PCD. The points of carbonate release and rebinding are unknown and are shown only to complete the stoichiometry of the reaction.

the deprotonation of PCA hydroxyl functions, whereas OH^- and the tyrosinate anion are ideally suited. The final step in substrate binding is predicted to be deprotonation of the PCA^{O3} which has a pK_a of ≈11.7 (*46*). This step would be poorly catalyzed by either bicarbonate (formed after deprotonation of the PCA^{O4}) or positively charged histidine predicted from the hydrogen bonding pattern observed in the crystal structure (see Figure 11), and thus, it might occur very slowly, as observed. The protonation of the tricarboxylic acid product would be a significantly more facile process and could be promoted more readily by the protonated forms of the bases available. Thus, although the process of product dissociation is slowed significantly, its rate is decreased much less than that of the substrate binding, and therefore, it is no longer the rate-limiting step in catalysis.

It is postulated that the ring-opening process involves generation of product in the *cis*,*cis* conformation adjacent to vacant sites in the iron coordination. Consequently, it is reasonable that a bidentate product chelate of the iron is formed as an intermediate, possibly ESO_2*. If, in Y447H, the two carboxylate−Fe^{3+} bonds are broken at significantly different rates due to different rates of protonation, an intermediate with only one carboxylate bound to the iron would be expected to form. This intermediate, perhaps ESO_2**, would probably have a single carboxylate ligand to the iron instead of the carbonate ligand of the resting enzyme, but the nature of the iron ligands, and thus the optical spectra, would be similar, as observed. The scheme in Figure 13 summarizes the proposal for the mechanism of Y447H and, by extension, all Fe^{3+} dioxygenases that emerge from the analysis of our observations discussed here.

Conclusion. We have used the first site-directed mutation of an Fe^{3+} dioxygenase to show that the novel ligand dissociation of Tyr447 is important to catalysis, and that it specifically affects the substrate binding and product release steps in ways that are consistent with our previous mechanistic proposals. Specifically, the most direct interpretation of the observations is that the principal role of the ligand dissociation is to generate an active site base to facilitate the binding of PCA as a dianion that can be attacked directly by O_2. The availability of a mutagenesis system that yields active enzymes with little overall structural change will be useful in the study of other aspects of the catalyzed reaction, including the influence of the nondissociating ligands to the iron and the roles of other active site residues. The contribution to catalysis of metal ligands dynamically dissociating and reassociating during the reaction cycle has not been widely explored in biological system. The studies described here are the first to examine the details of such a process and demonstrate that its disruption profoundly affects the efficiency of turnover. It is likely that similar mechanistic strategies are applied by other metalloenzymes as a means of unmasking nucleophilic reagents at the time required during the catalytic cycle.

ACKNOWLEDGMENT

We thank Jeremy C. Nesheim and Sang-Kyu Lee for assistance in making the transient kinetic measurements reported here.

REFERENCES

1. Lipscomb, J. D., and Orville, A. M. (1992) in *Metal Ions in Biological Systems* (Sigel, H., and Sigel, A., Eds.) pp 243−298, Marcel Dekker, New York.
2. Que, L., Jr. (1989) in *Iron Carriers and Iron Proteins* (Loehr, T. M., Ed.) pp 467−524, VCH, New York.
3. Que, L., Jr. (1993) in *Bioinorganic Catalysis* (Reedijk, J., Ed.) pp 347−393, Marcel Dekker, New York.
4. Que, L., Jr., and Ho, R. Y. N. (1996) *Chem. Rev. 96*, 2607−2624.

5. Ohlendorf, D. H., Lipscomb, J. D., and Weber, P. C. (1988) *Nature 336*, 403−405.
6. Ohlendorf, D. H., Orville, A. M., and Lipscomb, J. D. (1994) *J. Mol. Biol. 244*, 586−608.
7. Orville, A. M., Lipscomb, J. D., and Ohlendorf, D. H. (1997) *Biochemistry 36*, 10052−10066.
8. Ferrin, T. E., Huang, C. C., Jarvis, L. E., and Langridge, R. (1988) *J. Mol. Graphics 6*, 13−27.
9. Siu, D. C., Orville, A. M., Lipscomb, J. D., Ohlendorf, D. H., and Que, L., Jr. (1992) *Biochemistry 31*, 10443−10448.
10. Orville, A. M., Elango, N., Lipscomb, J. D., and Ohlendorf, D. H. (1997) *Biochemistry 36*, 10039−10051.
11. Elgren, T. E., Orville, A. M., Kelly, K. A., Lipscomb, J. D., Ohlendorf, D. H., and Que, L., Jr. (1997) *Biochemistry 36*, 11504−11513.
12. Feig, A. L., and Lippard, S. J. (1994) *Chem. Rev. 94*, 759−805.
13. Wallar, B. J., and Lipscomb, J. D. (1996) *Chem. Rev. 96*, 2625−2657.
14. Schindelin, H., Kisker, C., Hilton, J., Rajagopalan, K. V., and Rees, D. C. (1996) *Science 272*, 1615−1621.
15. Lah, M. S., Dixon, M. M., Pattridge, K. A., Stallings, W. C., Fee, J. A., and Ludwig, M. L. (1995) *Biochemistry 34*, 1646−1660.
16. Roach, P. L., Clifton, I. J., Hensgens, C. M. H., Shibata, N., Schofield, C. J., Hajdu, J., and Baldwin, J. E. (1997) *Nature 387*, 827−830.
17. Fülöp, V., Moir, J. W. B., Ferguson, S. J., and Hajdu, J. (1995) *Cell 81*, 369−377.
18. Williams, P. A., Fülöp, V., Garman, E. F., Saunders, N. F. W., Ferguson, S. J., and Hajdu, J. (1997) *Nature 389*, 406−412.
19. Gerischer, U., and Ornston, L. N. (1995) *J. Bacteriol. 177*, 1336−1347.
20. Frazee, R. W., Livingston, D. M., LaPorte, D. C., and Lipscomb, J. D. (1993) *J. Bacteriol. 175*, 6194−6202.
21. Fox, B. G., Froland, W. A., Dege, J., and Lipscomb, J. D. (1989) *J. Biol. Chem. 264*, 10023−10033.
22. Embretson, J. E., and Livingston, D. M. (1984) *Gene 29*, 293−302.
23. Boyer, H. W., and Roulland-Dussoix, D. (1969) *J. Mol. Biol. 41*, 459−472.
24. Figurski, D. H., and Helinski, D. R. (1979) *Proc. Natl. Acad. Sci. U.S.A. 76*, 1648−1652.
25. Yen, K. M. (1991) *J. Bacteriol. 173*, 5328−5335.
26. Cohen-Bazire, G., Sistrom, W. R., and Stanier, R. Y. (1957) *J. Cell. Comp. Physiol. 49*, 25−68.
27. Sanger, F., Nicklen, S., and Coulsen A. R. (1977) *Proc. Natl. Acad. Sci. U.S.A. 74*, 5463−5467.
28. Sambrook, J., Fritsch, E. F., and Maniatis, T. (1989) in *Molecular Cloning: a Laboratory Manual*, 2nd ed., Cold Spring Harbor Laboratory Press, Cold Spring Harbor, NY.
29. Laemmli, U. K. (1970) *Nature 227*, 680−681.
30. MacDonald, D. L., Stanier, R. Y., and Ingraham, J. L. (1954) *J. Biol. Chem. 210*, 809−820.
31. Lee, S.-K., Nesheim, J. C., and Lipscomb, J. D. (1993) *J. Biol. Chem. 268*, 21569−21577.
32. Hendrickson, W. A., and Konnert, J. H. (1980) in *Biomolecular Structure, Function, Conformation and Evolution* (Srinvasan, R., Ed.) Vol. 1, pp 43−47, Pergamon, Oxford.
33. Hendrickson, W. A. (1985) *Methods Enzymol. 115*, 252−270.
34. Hooft, R. W. W., Vriend, G., Sander, C., and Abola, E. E. (1996) *Nature 381*, 272.
35. Kraulis, P. J. (1991) *J. Appl. Crystallogr. 24*, 946−950.
36. Arnez, J. G. (1994) *J. Appl. Crystallogr. 27*, 649−653.
37. Ornston, L. N., and Stanier, R. Y. (1966) *J. Biol. Chem. 241*, 3776−3786.
38. Whittaker, J. W., Orville, A. M., and Lipscomb, J. D. (1990) *Methods Enzymol. 188*, 82−88.
39. Fujisawa, H., and Hayaishi, O. (1968) *J. Biol. Chem. 243*, 2673−2681.
40. Fujisawa, H., Hiromi, K., Uyeda, M., Okuno, S., Nozaki, M., and Hayaishi, O. (1972) *J. Biol. Chem. 247*, 4422−4428.
41. Bull, C., Ballou, D. P., and Otsuka, S. (1981) *J. Biol. Chem. 256*, 12681−12686.
42. Luzzati, V. (1952) *Acta Crystallogr. 5*, 802−810.
43. Kurokawa, H., Mikami, B., and Hirose, M. *(1995) J. Mol. Biol. 254*, 196−207.
44. Day, C. L., Anderson, B. F., Tweedie, J. W., and Baker, E. N. (1993) *J. Mol. Biol. 232*, 1084−1100.
45. Whittaker, J. W., and Lipscomb, J. D. (1984) *J. Biol. Chem. 259*, 4476−4486.
46. Smith, R. H., and Martell, A. E. (1989) in *Critical Stability Constants* (Suppl. 2 and earlier volumes), Vol. 6, Plenum Press, New York.

BI972047B